https://doi.org/10.1016/j.apacoust.2017.05.034

Optimization of geometrical parameters for a supporting structure with two installed coherent machines

Zhen Wang [a], Cheuk Ming Mak [a,*], Dayi Ou [b,c]

[a] Department of Building Services Engineering, The Hong Kong Polytechnic University, Hung Hom, Kowloon, Hong Kong, China

[b] School of Architecture, Huaqiao University, Xiamen, 361021, China

[c] State Key Laboratory of Subtropical Architecture Science, South China University of Technology, Guangzhou 510640, China

*Corresponding Author: Tel.: +852 2766 5856; Fax: +852 2765 7198

E-Mail: cheuk-ming.mak@polyu.edu.hk (C.M. Mak)

ABSTRACT: It is common to have two or more vibratory machines of the same type mounted on the same supporting structure. These vibratory machines transmit structure-borne sound to adjacent walls or floors and the structure-borne sound is eventually emitted as noise into indoor spaces. The interactions of the mounting points among coherent machines increase the structure-borne sound power transmission significantly at some frequencies and decrease it considerably at some other frequencies. However, there is still no general design frameworks of supporting structure optimization strategy that target on minimizing structure-borne sound power transmission by utilizing the interactions of the mounting points among coherent machines properly. This paper for the first time develops a practical design framework to obtain an optimal set of geometrical parameters for a supporting structure by using a genetic algorithm with parametric finite element models. A steel-made supporting structure with two coherent

fans installed on were analyzed. Experiments were conducted to obtain the source mobilities and free velocities of the coherent fans that are required for the calculation of structure-borne sound power transmission. Parametric finite element analysis was conducted to obtain the receiver mobility of the supporting structure. A genetic algorithm solved the optimal solution. The results shown that the proposed approach is sufficiently capable of minimizing the structure-borne sound power transmission on a supporting structure with coherent machines mounted on a supporting structure.

Keywords: Structure-borne sound transmission; Vibratory machines; Genetic algorithms; Geometry optimization;

1. Introduction

Vibratory machines such as boilers, chillers, pumps, electric motors, air compressors, fans, and generators are installed in buildings. These vibratory machines produce direct mechanical excitation to floors and walls that is finally emitted as an unwanted sound into indoor spaces. Noise and vibration can produce serious problems to residents. These problems cause annoyance to occupants [1, 2], negatively affect job performance [3], and increase health risks [4]. To provide quiet and comfortable working and living spaces, any techniques that can decrease noise and vibration levels by a few decibels are meaningful to be utilized. As one of the most feasible and commercially applicable ways, vibration isolators are widely adopted by engineers.

In practice, the dimensionless isolation efficiency of vibration isolators is assessed by the force transmissibility method or motion transmissibility method [5]. Mak and Su [6-8] pointed

out that the structure-borne sound power transmission appears to be more viable than the transmitted forces of motion between the complex vibratory source and the receiving floor structure. They then proposed the “power transmissibility” method to evaluate the performance of vibration isolators. Structure-borne sound power transmission of a machine can be measured by the direct method [9], indirect method [10] and the mobility method [11-17]. The mobility method can be adopted to calculate a machine’s structure-borne sound power transmission conveniently. Mak and Yun [18, 19] adopted the mobility method in analyzing the structure-borne sound power transmission of two coherent machines to a simple floor structure and a dual-layer coupling floor structure. Their analyzed results showed that the power obtained from the two coherent machines could differ considerably from that obtained from independent machines at some frequencies. They pointed out that the reason for the differences were the existence of the coupling effect due to the interactions of the mounting points among the two coherent machines.

The coupling effect results in structure-borne sound power transmission of coherent machines that is magnified at some frequencies and decreased at some other frequencies. The coupling effect can therefore be utilized to reduce the structure-borne sound power transmission of coherent machines at targeted frequencies. Synchrophasing control [20, 21] is a kind of control technique that works in this way. Synchrophasing control can be dated back to 1980s and was first studied in controlling propeller noise of aircraft. This technique has been recently introduced in vibration control area. Dench et al. [22] investigated vibration transmission from two coherent vibration sources to a structure minimized by synchrophasing control theoretically and experimentally. Synchrophasing control technique reduces noise and vibration by utilizing

the interactions of coherent noise and vibration sources. However, to the best of the authors' knowledge, utilization of interactions of the mounting points among coherent machines has not been reported in the published literature. This paper therefore targeted on utilizing the interaction of mounting points among coherent machines properly by developing a practical geometry optimization approach. This optimization approach can obtain a set of geometrical parameters for the supporting structure of coherent machines. The genetic algorithm (GA) and parametric finite element analysis (FEA) models are utilized in the geometry optimization of supporting structures.

As shown in Fig. 1, a supporting structure with two coherent fans mounted, was considered in this paper. Source mobility and free velocities of the fans, receiver mobility of the supporting structure should be determined so as to obtain the transmitted structure-borne sound power. Free velocities and source mobilities of the fans were measured by experiments in this study. Receiver mobility of the supporting structure was obtained by parametric FEA models. A set of receiver mobility obtained by parametric FEA models was validated by experimental measurements.

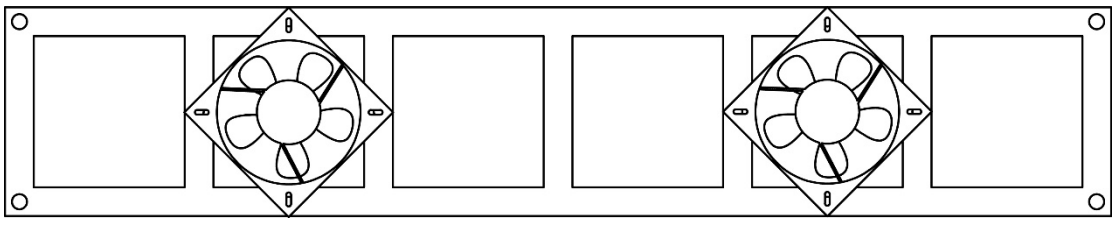

Fig. 1. A schematic diagram of the supporting structure with two coherent fans mounted.

2. The structure-borne sound power transmission

Considering the supporting structure without fans mounted, as shown in Fig. 2 with the rectangular coordinate system OXY attached. Points 1-4 are mounting points for one fan, and points 5-8 are mounting points for another fan. The dimensions for this supporting structure are: length L, width W, and thickness d. The widths of the upper beam and the lower beam paralleled to the X-axis in the rectangular coordinate system as shown in Fig. 2, are w_1 and w_2, respectively. The width of each of the seven beams paralleled to the Y-axis in the rectangular coordinate system as shown in Fig. 2 is w_3.

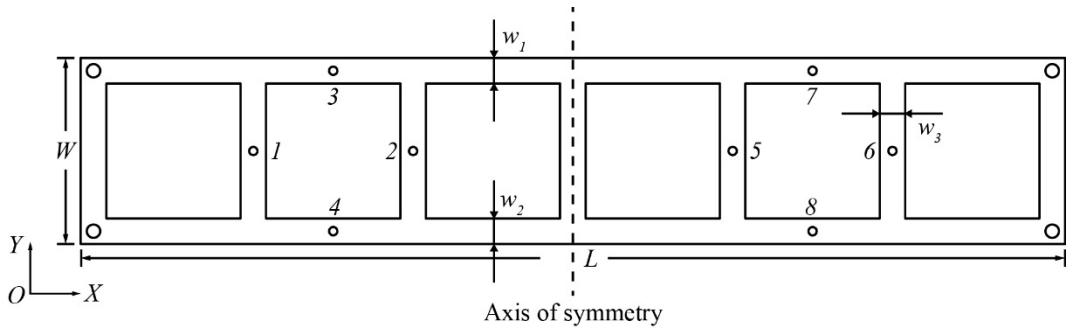

Fig. 2. A schematic diagram of the supporting structure.

The structure-borne sound power transmitted from the two coherent fans to the supporting structure, is selected as the fitness function in this study. Thus, the structure-borne sound power transmission should be calculated. It starts with calculating the transmitted force.

Assuming that the free velocity vectors of the fans are given by:

$$\left[v_{fi} \right] = [v_{i1}, v_{i2}, v_{i3}, v_{i4}]^T \qquad i = 1, 2 \tag{1}$$

where the superscript T denotes the transpose of a matrix, i stands for the numbers of the fans, 1-4 in the right part of the equation stand for the four mounting points on each fan.

The dynamic force transmitted from two coherent fans (with the coupling effect) and two independent fans (without the coupling effect) to the supporting structure at the eight mounting points, are given by:

$$[F_{Tc}]=\left(\begin{bmatrix} Y_{S1} & O \\ O & Y_{S2} \end{bmatrix}+\begin{bmatrix} Y_{R11} & Y_{R12} \\ Y_{R21} & Y_{R22} \end{bmatrix}\right)^{-1}\begin{bmatrix} v_{f1} \\ v_{f2} \end{bmatrix} \tag{2}$$

$$[F_{Ti}]=\left(\begin{bmatrix} Y_{S1} & O \\ O & Y_{S2} \end{bmatrix}+\begin{bmatrix} Y_{R11} & O \\ O & Y_{R22} \end{bmatrix}\right)^{-1}\begin{bmatrix} v_{f1} \\ v_{f2} \end{bmatrix} \tag{3}$$

where O is the null matrix, $[Y_{S1}]$ and $[Y_{S2}]$ denotes the source mobility matrices of the two fans, are given by:

$$[Y_{S1}]=\begin{pmatrix} Y_{sm11} & Y_{sm12} & Y_{sm13} & Y_{sm14} \\ Y_{sm21} & Y_{sm22} & Y_{sm23} & Y_{sm24} \\ Y_{sm31} & Y_{sm32} & Y_{sm33} & Y_{sm34} \\ Y_{sm41} & Y_{sm42} & Y_{sm43} & Y_{sm44} \end{pmatrix}, \text{ and } [Y_{S2}]=\begin{pmatrix} Y_{sm55} & Y_{sm56} & Y_{sm57} & Y_{sm58} \\ Y_{sm65} & Y_{sm66} & Y_{sm67} & Y_{sm68} \\ Y_{sm75} & Y_{sm76} & Y_{sm77} & Y_{sm78} \\ Y_{sm85} & Y_{sm86} & Y_{sm87} & Y_{sm88} \end{pmatrix} \tag{4}$$

$$[Y_{R11}]=\begin{pmatrix} Y_{rm11} & Y_{rm12} & Y_{rm13} & Y_{rm14} \\ Y_{rm21} & Y_{rm22} & Y_{rm23} & Y_{rm24} \\ Y_{rm31} & Y_{rm32} & Y_{rm33} & Y_{rm34} \\ Y_{rm41} & Y_{rm42} & Y_{rm43} & Y_{rm44} \end{pmatrix}, \text{ and } [Y_{R12}]=\begin{pmatrix} Y_{rm15} & Y_{rm16} & Y_{rm17} & Y_{rm18} \\ Y_{rm25} & Y_{rm26} & Y_{rm27} & Y_{rm28} \\ Y_{rm35} & Y_{rm36} & Y_{rm37} & Y_{rm38} \\ Y_{rm45} & Y_{rm46} & Y_{rm47} & Y_{rm48} \end{pmatrix} \tag{5}$$

$$[Y_{R21}]=\begin{pmatrix} Y_{rm51} & Y_{rm52} & Y_{rm53} & Y_{rm54} \\ Y_{rm61} & Y_{rm62} & Y_{rm63} & Y_{rm64} \\ Y_{rm71} & Y_{rm72} & Y_{rm73} & Y_{rm74} \\ Y_{rm81} & Y_{rm82} & Y_{rm83} & Y_{rm84} \end{pmatrix}, \quad \text{and} \quad [Y_{R22}]=\begin{pmatrix} Y_{rm55} & Y_{rm56} & Y_{rm57} & Y_{rm58} \\ Y_{rm65} & Y_{rm66} & Y_{rm67} & Y_{rm68} \\ Y_{rm75} & Y_{rm76} & Y_{rm77} & Y_{rm78} \\ Y_{rm85} & Y_{rm86} & Y_{rm87} & Y_{rm88} \end{pmatrix}$$

(6)

$[Y_{R11}]$ denotes the mobility matrix of the mounting points 1-4 (for installing the first fan) on the supporting structure, and $[Y_{R12}]$ denotes the mobility matrix between the mounting points 1-4 and the mounting points 5-8 (for installing the second fan) on the supporting structure. The schematic diagram of the supporting structure has a bilateral symmetry, with left and right parts as mirror images of each other, as shown in Fig. 2. For topological mirror image symmetry between mounting points 1-4 and mounting points 5-8, $[Y_{R21}]= [Y_{R12}]^{T}$ denotes the mobility matrix between the mounting points 5-8 and the mounting points 1-4 on the supporting structure, $[Y_{R22}]=[Y_{R11}]$ denotes the mobility matrix of the mounting points 5-8 on the supporting structure.

The structure-borne sound powers transmitted from two coherent fans and two independent fans to the supporting structure are given by [23]:

$$P_c = \frac{1}{2} R\mathrm{e}\left([F_{Tc}]^{*\mathrm{T}} \begin{bmatrix} Y_{R11} & Y_{R12} \\ Y_{R21} & Y_{R22} \end{bmatrix} [F_{Tc}] \right) \tag{7}$$

$$P_i = \frac{1}{2} R\mathrm{e}\left([F_{Ti}]^{*\mathrm{T}} \begin{bmatrix} Y_{R11} & O \\ O & Y_{R22} \end{bmatrix} [F_{Ti}] \right) \tag{8}$$

The asterisk denotes the complex conjugate. Refer to the equations 1 to 8, the source quantities (free velocities and source mobilities) of the fans and the receiving mobility of the supporting structure should be obtained to calculate the structure-borne sound power transmission. In this study, the source quantities were obtained by experimental measurement, whilst the receiver mobility of the supporting structure was obtained by parametric FEA model.

3. Parametric Finite Element Analysis

The commercial FEA software COMSOL was utilized for the structural mechanics simulation in this study. A COMSOL FEA model is convenient to be set-up within the MATLAB scripting environment. Thus, by writing and running a MATLAB routine with parameters of geometry sizes being defined, the corresponding parametric FEA models can be set-up.

A supporting structure as shown in Fig. 2 is manufactured, with medium carbon steel. The sizes for this supporting structure are length L=0.77m, width W=0.145m and thickness d=0.004m. The widths of the upper and lower beam paralleled to the X-axis in the rectangular coordinate system as shown in Fig. 2 are $w_1 = w_2 = 0.02m$. The width of each of the seven beams paralleled to the Y-axis in the rectangular coordinate system as shown in Fig. 2 is $w_3 = 0.02m$.

The material properties for the supporting structure are density ρ=7.8×10^3kg/m^3, Young's modulus E=2.1×10^{11}N/m^2, Poisson's factor μ=0.269 and isotropic loss factor η=0.01. The frequency band between 5Hz and 200Hz was analyzed.

The supporting structure was fixed to a floor through the four holes on the corners of the supporting structure with steel screws. In the parametric FEA models, the floor of which the supporting structure mounted on was assumed rigid and non-movable. Therefore, the four holes on the corners of the supporting structure were set to be fixed on all directions. To get closer to the real condition, the gravity load was also considered in the FEA model. The gravity load on the supporting structure was the dead weight of the supporting structure.

In the parametric FEA model, the tetrahedral elements were utilized. In order to obtain a more accurate result, a finer mesh was defined in the element size list of COMSOL than the default setting suggested. High quality elements were created with a regular tetrahedral mesh generation method.

In a FEA model, a constant externally applied force load was defined on point 6 with frequency sweeping from 5Hz to 200Hz, the increment was 1Hz. By conducting frequency modal analysis, the frequency response of velocity at each point on the geometry of the supporting structure was solved. Dividing velocity by the correspondent force load, the mobility was obtained. The transfer mobility between point 6 and point 1 and the transfer mobility between point 6 and point 2 were taken as examples, which are presented in Fig. 3 as magnitudes.

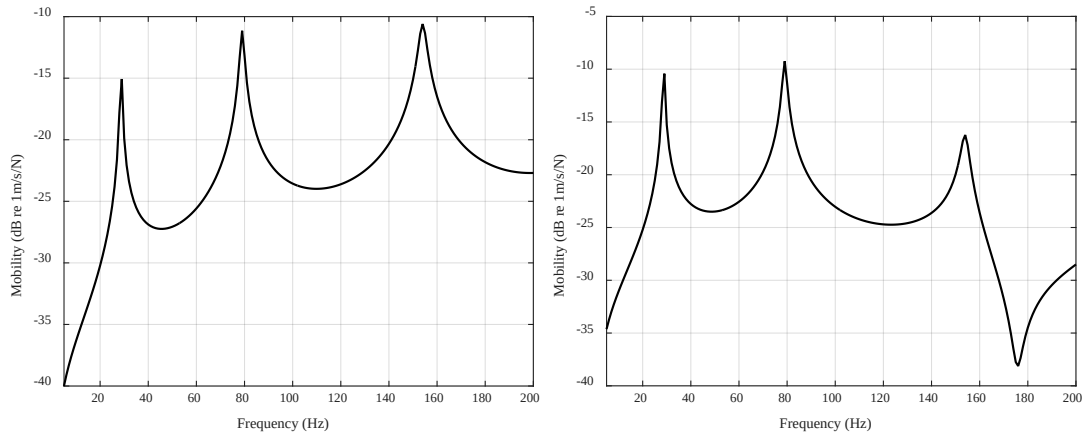

(a) (b)

Fig. 3. (a) Magnitude of the transfer mobility between point 6 and point 1; (b) magnitude of the transfer mobility between point 6 and point 2.

4. Experimental works

The experimental works involve measurements of the fans and the supporting structure. Measurements of the fans are to obtain the source characterization: free velocities and source mobilities of the fans. Measurement of the supporting structure is to obtain receiver mobility of the supporting structure and compare with simulation results of COMSOL FEA models. The experimental procedures of measuring the source mobility and receiver mobility were based on the Standards ISO7626-1 [24] and ISO7626-5 [25]. In the experiments, only the vibration in the vertical direction – the Z axis in the natural coordinate system was considered.

4.1. Free velocities of the fans

One fan in this study was hang by elastic ropes, as shown in Fig. 4 with the natural coordinate system OXYZ attached. With the fan in operation, the free velocity at the four mounting points were collected by Brüel & Kjær type 4394 accelerometers. The vertical view of the fan with four accelerators mounted on the four points is show in Fig. 5. The free

accelerations were sampled by Brüel & Kjær Pulse 3560B. Consequently, Brüel & Kjær Labshop integrate accelerations to velocities and record the velocity data. The recorded velocity data as complex values with frequency resolution of 1Hz and frequency band of 5Hz-200Hz was analyzed. The magnitude of velocity at the four mounting points are presented in Fig. 6. Refer to Fig. 6, it can be discerned that magnitude of free velocity in the frequency band below 50 Hz are significant larger than magnitude of free velocity in other frequency bands.

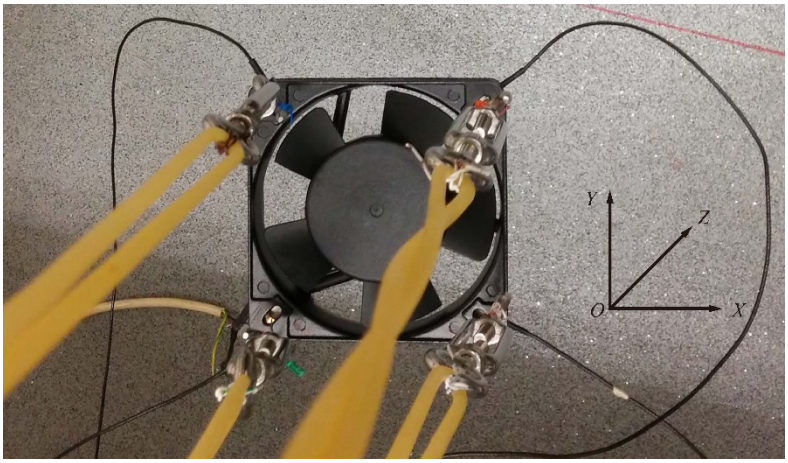

Fig. 4. Picture of the fan hang by elastic robes.

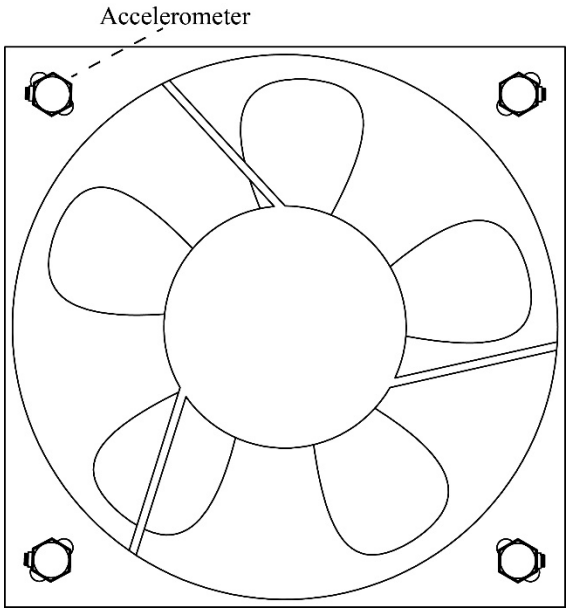

Fig. 5. A vertical view of one fan with four accelerators mounted.

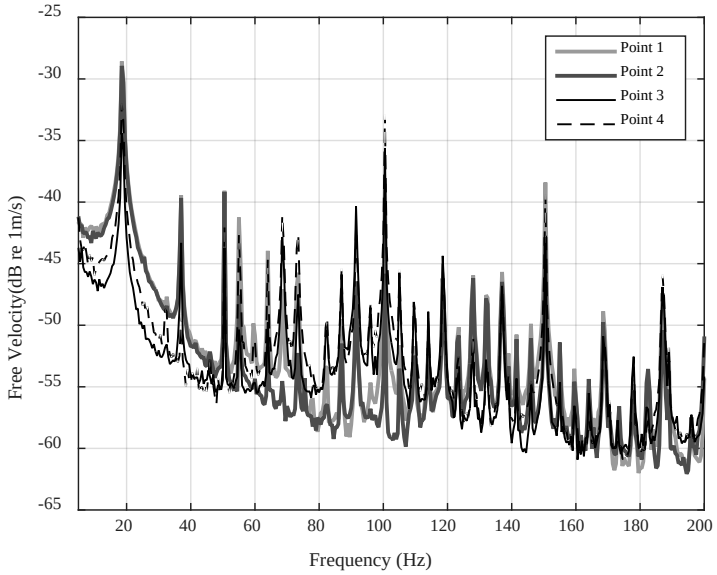

Fig. 6. Magnitude of free velocity at the four mounting points.

4.2. Source mobilities of the fans

The complex source mobility measurement was conducted by using a KISTLER type 9276A force hammer with in-line force transducer and accelerometer, with the fan suspended with elastic ropes. The force and acceleration were sampled and recorded by Brüel & Kjær Pulse 3560B and Labshop. The instrumentation system is presented schematically in Fig. 7. In Labshop, the measurements were started up with trigger excitation, different from most measurements, which do not need to set star-up styles. The acceleration data was integrated into velocity data in Brüel & Kjær Labshop. The source mobility was then calculated by dividing force to velocity. For each source mobility, 10 measures were conducted and then averaged. Fig. 8 shows the magnitude of averaged point mobility at the four mounting points on the fan.

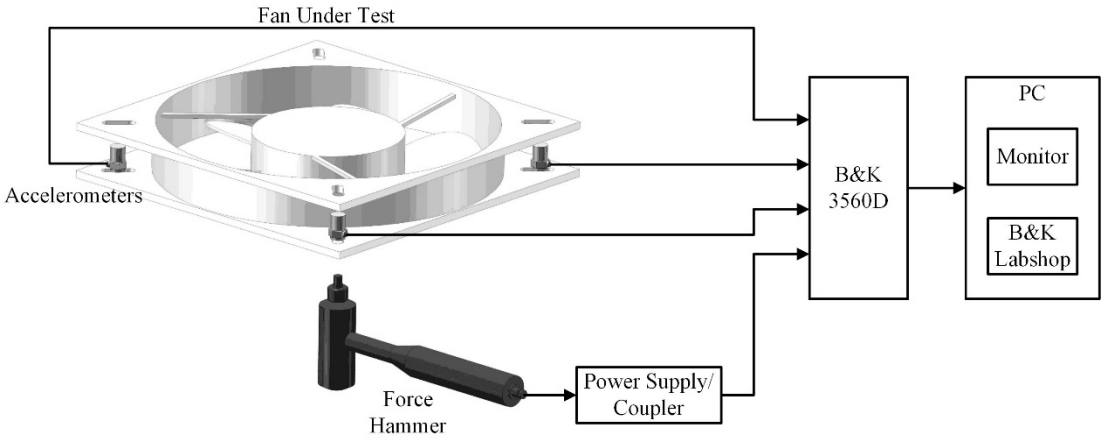

Fig. 7. Instrumentation block diagram for source mobility measurement

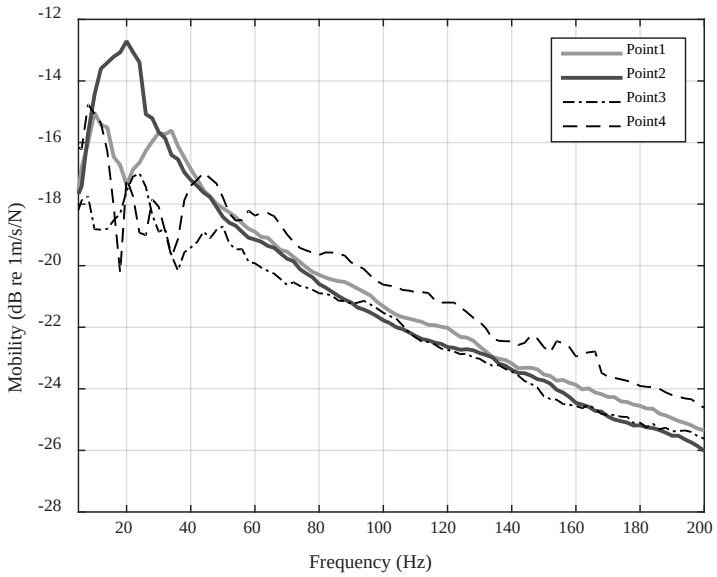

Fig. 8. Magnitude of averaged point mobility at the four mounting points on the fan

4.3. Receiver mobility of the supporting structure

The complex receiver mobility was recorded using a force hammer with in-line force transducer and accelerometer, similar to the procedure mentioned in section 4.2, with the supporting structure installed fixed on the floor. The connection between the structure and the floor was through the four holes on the corners of the supporting structure with steel screws. The force applied and acceleration response were recorded as complex value. The acceleration

data was integrated into velocity data in Brüel & Kjær Labshop. The source mobility was then calculated by dividing force to velocity. For each source mobility, 10 measures were conducted and then averaged.

To validate results solved by FEA model, FEA results were compared with measured results of mobility on the supporting structure. The magnitude of the measured transfer mobility between point 6 and point 1 is plotted with dashed line in Fig. 9 (a) and the magnitude of the measured transfer mobility between point 6 and point 2 is plotted with dashed line Fig. 9 (b). The corresponding FEA results are plotted with solid lines in Fig. 9.

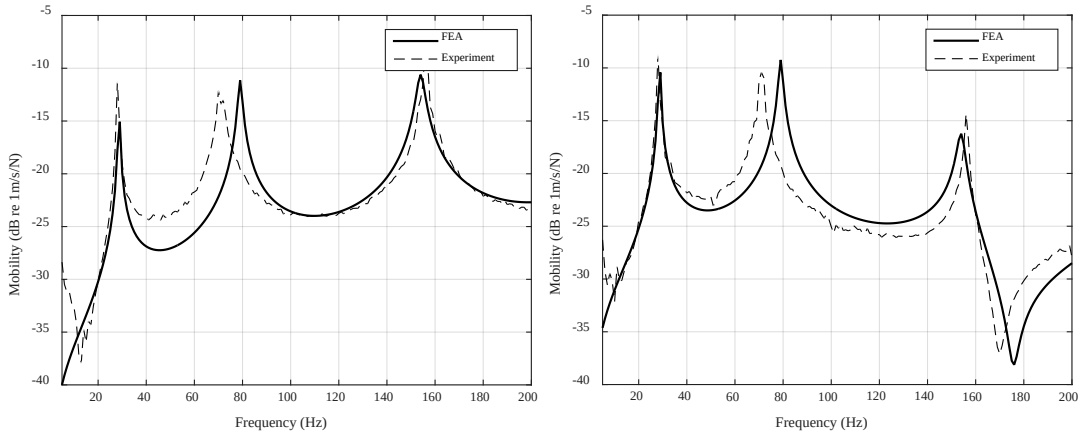

(a) (b)

Fig. 9. (a) Magnitude of FEA and experiment results of transfer mobility between point 6 and point 1 on the supporting structure; (b) magnitude of FEA and experiment results of transfer mobility between point 6 and point 2 on the supporting structure.

It can be observed that the differences between FEA model results and experiment measurement results are small. Considering the existence of experimental errors, the differences between simulation results and the measurement results are acceptable. Thus, FEA simulation results of mobility are acceptable. The FEA parametric models are suitable for the optimization process.

5. The GA Optimization Process

GAs have been applied to a wide range of applications in economics, mechanics, computer science, mathematics, and engineering for their significant advantages. One significant advantage of GAs is the capability to handle multiple solution search spaces simultaneously. Another noticeable advantage of GAs is their suitability for problems with variables in discrete data series. With these two significant advantages, GAs are quite suitable for the optimization process in this study.

The GAs are adopted to search optimal solutions, which are inspired by the process of natural selection and evaluation [26]. The basic concept of a GA is to generate the optimal individuals, also known as the genes, which fit the requirement of the fitness function best through evaluation of several generations. It starts with generating the initial population randomly. Then, an iteration process is applied to make the population evaluate towards global optimal. At each generation, “parents” among the individuals of the current generation which have the best fitness value were selected. These selected “parents” are utilized to generate “children” that will constitute the population for the next generation. For most GAs, four bio-inspired operators: evaluation, selection, crossover, and mutation are utilized. All these four operators are analogue to their corresponding biological generation operation.

Evaluation operator weights the fitness of each individuals in the current generation. The fitness, calculated by the fitness function, indicate the quality of individuals. Selection operator selects excellent individuals in the current generation for breeding the next generation individuals. Crossover operator changes the binary data of chromosomes from one generation

to the next generation. Mutation operator changes one or more gene value in a chromosome for individuals in the next generation.

In this study, a package of GA code was utilized for the optimization process, as shown in Fig. 10. Before the optimization process started, several GA option information such as the population size and the individual size should be defined. Besides, the optimization parameters, bounds, constraints, and most importantly, the fitness function should also be defined. Then, these codes can automatically proceed all operations required by GAs included initial population, evaluation, selection, crossover, mutation, and elitism.

Each individual in a population was represented by a binary vector. Each vector contains binary data of the three design parameters which defined a supporting structure. To evaluate an individual, a MATLAB subroutine passed the corresponding binary vector to a COMSOL server automatically. The COMSOL server generated a parametric FEA model with the corresponding optimization parameters. Frequency modal analysis of velocity response was studied consequently. Thus, the receiver mobility can be calculated and passed to the main optimization routine.

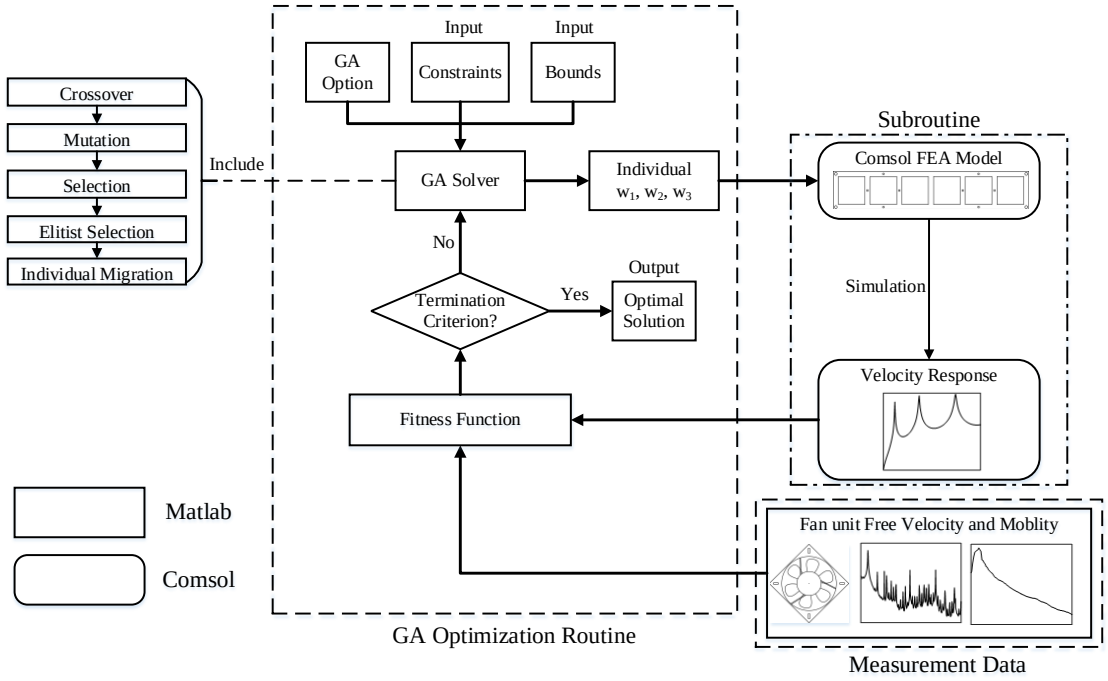

Fig. 10. Diagram of the optimization algorithm routine.

5.1. The GA option

The genetic algorithm option information included the population size, individual size, rate of immigration, interval of migration, rate of crossover and rate of mutation were specified before the optimization process. In this study, the population size, M was 10; the individual size, N was 20; the interval of migration, G was a random decimal number between 0.3 and 0.9 which automatically generated in the optimization routine; the rate of crossover, R_c was a randomly generated decimal number between 0.4 and 0.99; the rate of mutation, R_m was a randomly generated decimal number between 0.0001 and 0.1. The maximum number of generations (iterations), M_g was 10 in this study, which is the maximum possible number of iterations the GA executes without the optimization having reached convergence.

5.2. Optimization design parameters

There were three design parameters that defined the dimensions of the supporting structure considered in the optimization process, that were the width of the upper beam paralleled to the *X*-axis in the rectangular coordinate system as shown in Fig. 2, w_1; the width of the lower beam paralleled to the *X*-axis in the rectangular coordinate system as shown in Fig. 2, w_2; the width of each of the steels paralleled to the *Y*-axis in the rectangular coordinate system as shown in Fig. 2, w_3. The upper and lower bounds, increment and number of possible cases for each design parameter are presented in Table 1.

Table 1

Upper and lower bounds, increments and number of possible cases for each design parameter

Parameter	Lower Bound	Upper bound	Increment	Cases
w_1 *(mm)*	12.8	24.8	0.8	16
w_2 *(mm)*	12.8	24.8	0.8	16
w_3 *(mm)*	12.8	24.8	0.8	16

5.3 The fitness function

The fitness function as a part of the package of GA code was called during each evaluation step to weight the quality of individuals. In this study, the optimal supporting structure geometry design would be the one with the minimal structure-borne sound power transmission of the two coherent fans. Therefore, the minimum structure-borne sound power transmission was taken as the fitness function, expressed as:

$$P_{fit} = \min(\mathrm{P}) \tag{8}$$

where *P* denotes the structural-borne sound power transmission of the two coherent fans.

6. Results and discussion

6.1. The structure-borne sound power transmission

With experimental results of free velocity, source mobility and receiver mobility, the structure-borne sound power transmission of the two coherent fans can be calculated by Eq. 7. The calculation result is present in Fig. 11. It is obvious, the frequency rang contains the largest power was frequencies below 60 Hz. For more specifically, 30 to 45 Hz (with magnitude larger than -60 dB) contains the largest magnitude of power. Although there are some other peaks near 100 Hz and 180 Hz, the magnitude increases and falls rapidly, covers a very small frequency range (about 3 Hz with magnitude larger than -60 dB). It is determined that the dominant frequency range of transmitted structure-borne sound power with the largest magnitude is 30Hz to 45 Hz. Thus, in the GA optimization process, the frequencies between 31Hz and 45 Hz was being focused on.

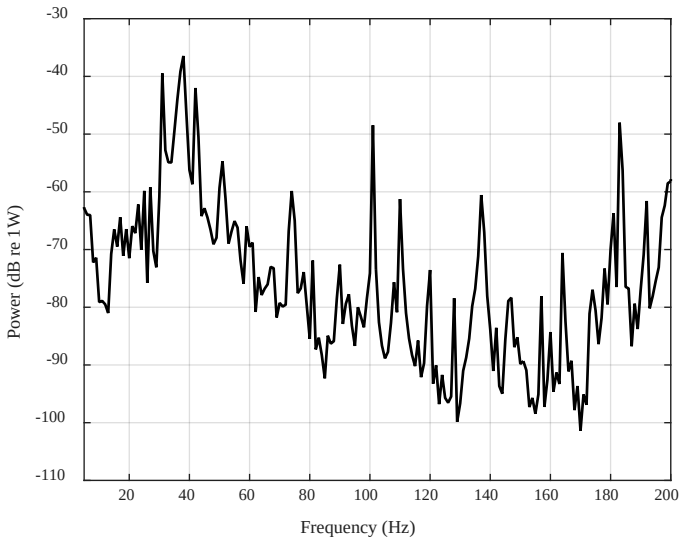

Fig. 11. Structure-borne sound power transmission from the two coherent fans to the supporting structure

6.2. Optimization of the supporting structure

The target of the optimization process was to minimize the structure-borne sound power transmission from the two coherent fans in the frequency range between 31 Hz and 45 Hz. Through the GA optimization process, the maximum value of the structure-borne sound power transmission decreased rapidly during the first few generation and converged gradually. The geometric parameters for the optimal design are w_1=0.0136, w_2=0.0128 and w_3=0.0192. The maximum magnitude of transmitted structure-borne sound power to the optimal supporting structure was -37.3dB. The structure-borne sound power transmission of the optimal design, the worst design and the original design between 31 Hz and 45 Hz are presented in Fig. 12. Refer to Fig. 12, the structure-borne sound power transmission of optimal design got a significant decrease of 9dB compared with the original design at 42Hz. The decrease of structure-borne sound power transmission at 35Hz was 3dB.

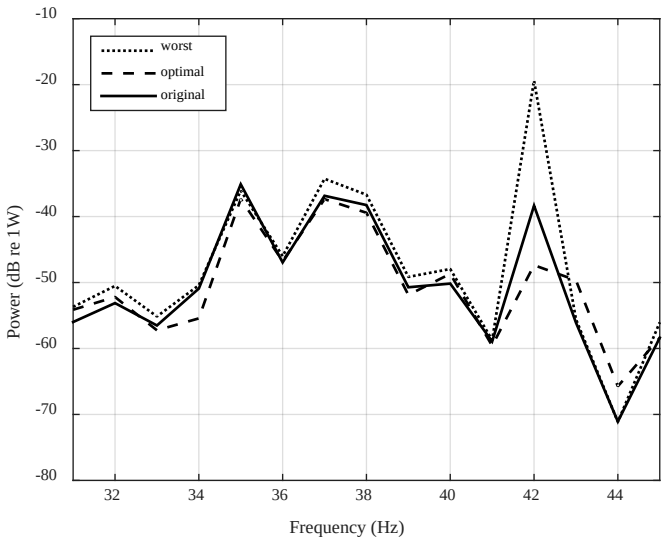

Fig. 12. Structure-borne sound power transmission of the supporting structures

For the supporting structure with the optimum parameters, the structure-borne sound power transmitted from the two coherent fans (with the coupling effect) and two independent

fans (without including the coupling effect) in the frequency band between 5Hz and 200Hz, are presented in Fig. 13. Fig. 13 illustrates that the structure-borne sound power transmission of two coherent fans is smaller than the structure-borne sound power transmitted of two independent fans in most regions of frequencies below 80 Hz. The decreases in structure-borne sound power transmission meet the target of reduce structure-borne sound power transmission at targeted frequencies by using the coupling effect.

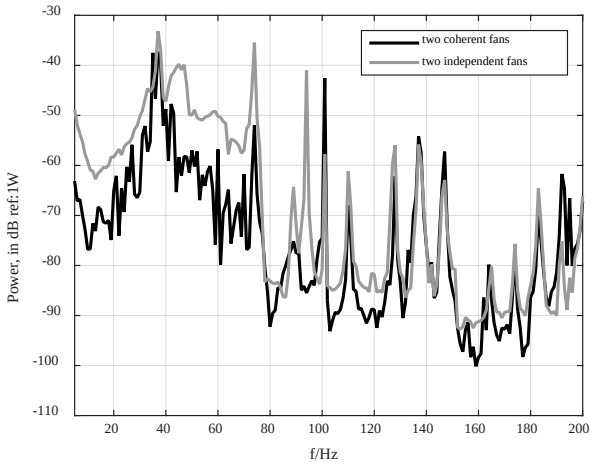

Fig. 13. Structure-borne sound power transmission of two coherent fans and two independent fans

After the optimization process, some more individuals were analyzed. The total amount of individuals being evaluated and recorded was 1800. The geometrical parameters and maximum magnitude of structure-borne sound power transmission of each individual (design) being evaluated is presented in Fig. 14.

Refer to Fig. 14, it shows that there exist some relationships between the geometrical parameters and the maximum magnitude of transmitted structure-borne sound power. Firstly, most of the individuals in the upper part have smaller magnitude of structure-borne sound power transmission than individuals in the lower part (refer to the differences of colors).

Therefore, it is concluded that individuals with larger value of parameter w_3 tend to obtain smaller structure-borne sound power transmission. Secondly, among individuals with the same value of parameters w_3 and w_1, individuals with smaller value of parameter w_2 tend to have smaller structure-borne sound power transmission. To present this relationship more specifically, individuals with parameter w_3 equals 0.0176 were presented in Fig. 15. It can be observed that, for individuals with the same value of parameter w_1, the smaller the parameter w_2 the smaller the magnitude of structure-borne sound power transmission (despite very little amount of random individuals do not obey this trend).

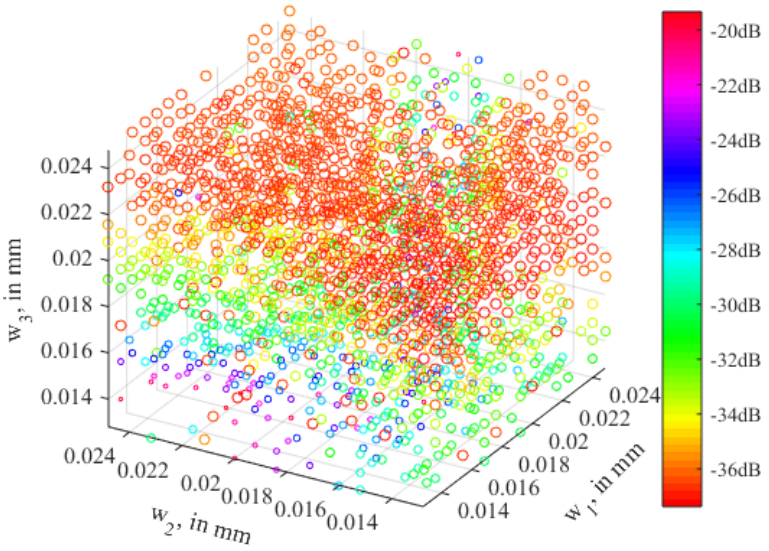

Fig. 14. (Color online) Maximum magnitude of structure-borne sound power transmission for each individual with their geometrical parameters w_1, w_2, and w_3

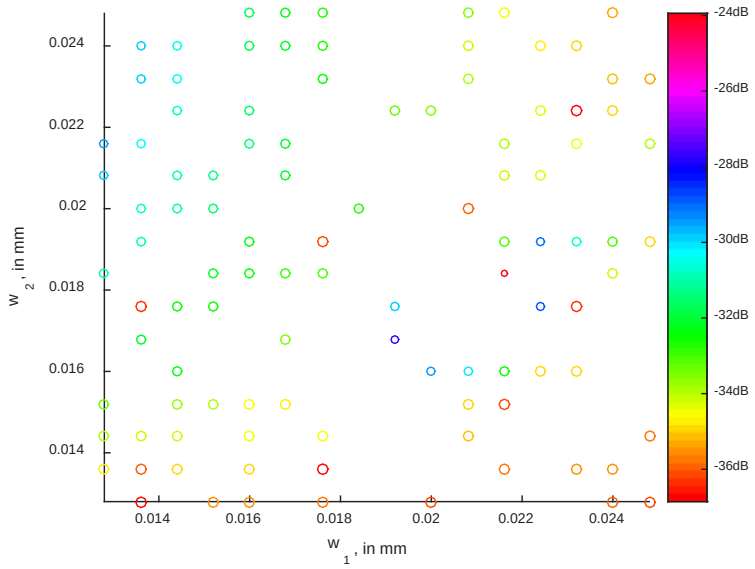

Fig. 15. (Color online) Plot of individuals which with the value of parameter w_3 equals 0.0176

Based on the results and analysis presented above, it can be concluded that the method utilized in this paper is effective. The following design framework for optimizing the geometrical parameters of a supporting structure with coherent machines installed can be provided:

a) Measure and record free velocities and source mobilities of the coherent machines;

b) Decide optimization parameters for the supporting structure which mounted the coherent machines;

c) Set up parametric FEA models of the supporting structure, for obtaining the receiver mobility;

d) Initiate the GA optimization routine and link it with the parametric FEA models;

e) Run the GA optimization routine and get the optima design.

7. Conclusions

Previous studies have shown that the coupling effect existed between coherent machines. Motivated by the existence of the coupling effect, this study attempted to decrease the structure-borne sound power transmission at selected frequencies with the help of the coupling effect. In this study, a GA-based optimization approach incorporated with parametric FEA models was proposed for obtaining optimal geometrical parameters of supporting structures.

A supporting structure with two coherent fans installed, as a case study, was analyzed in this study. Three geometrical parameters governing the size of a supporting structure were selected to be optimized. Experiments were conducted to measure free velocities and source mobilities of the fans. Parametric FEA models were utilized to obtain receiver mobility of the supporting structure. The structure-borne sound power transmission, calculated by utilizing the mobility method, was taken as the fitness function in the GA optimization process. The optimization results shown that the optimal design can obtain a decrease of about 18 dB in structure-borne sound power transmission, compared with the worst design. It is validated that the proposed optimization approach is effective in reducing the structure-borne sound power transmission of two coherent machines at targeted frequencies.

Acknowledgements

The authors would like to thank the financial support of the Hong Kong Polytechnic University. This work was also supported by the National Natural Science Foundation of China [grant number:51578252]; the State Key Lab of Subtropical Building Science, South China University of Technology [grant number: 2016ZB06].

References

[1] Ayr U, Cirillo E, et al. A new approach to assessing the performance of noise indices in buildings. Appl Acoust 2003;64(2):129-45.
[2] Mak CM, Wang Z. Recent advances in building acoustics: An overview of prediction methods and their applications. Build Environ 2015;91:118-26.
[3] Jahncke H. and Halin N. Performance, fatigue and stress in open-plan offices: The effects of noise and restoration on hearing impaired and normal hearing individuals. Noise Health 2012;14(60):260-72.
[4] Carletti E, Pedrielli F, Casazza C. Development and Validation of a Numerical Prediction Model to Estimate the Annoyance Condition at the Operation Station of Compact Loaders. Int J Occup Saf Ergonom 2011;17(3):233-40.
[5] Malcolm JC. Handbook of acoustics. New York: John Wiley & Sons; 1998.
[6] Mak CM, Su JX. A study of the effect of floor mobility on isolation efficiency of vibration isolators. J Low Freq Noise Vib Act Control 2001;20(1):1-13.
[7] Mak CM, Su JX. A study of the effect of floor mobility on structure-borne sound power transmission. Build Environ 2003;38(3):443-55.
[8] Mak CM, Su JX. A power transmissibility method for assessing the performance of vibration isolation of building services equipment. Appl Acoust 2002;63(12):1281-99.
[9] ISO 18312-1:2012. Mechanical vibration and shock - Measurement of vibration power flow from machines into connected support structures - Part 1: Direct method.
[10] ISO 18312-2:2012. Mechanical vibration and shock - Measurement of vibration power flow from machines into connected support structures - Part 2: Indirect method.
[11] Gibbs BM. Uncertainties in predicting structure-borne sound power input into buildings. J Acoust Soc Am 2013;133(5):2678-89.
[12] Moorhouse AT. Simplified calculation of structure-borne sound from an active machine component on a supporting substructure. J Sound Vib 2007;302(1-2):67-87.
[13] Moorhouse AT, Elliott AS, Evans TA. In situ measurement of the blocked force of structure-borne sound sources. J Sound Vib 2009;325(4-5):679-85.
[14] Ohlrich M. Predicting transmission of structure-borne sound power from machines by including terminal cross-coupling. J Sound Vib 2011;330(21):5058-76.
[15] Mayr AR, Gibbs BM. Point and transfer mobility of point-connected ribbed plates. J Sound Vib 2011;330(20):4798-812.
[16] Mayr AR, Gibbs BM. Single Equivalent Approximation for Multiple Contact Structure-Borne Sound Sources in Buildings. Acta Acust United Ac 2012;98(3):402-10.
[17] Yun Y, Mak CM. Assessment of the stability of isolated vibratory building services systems and the use of inertial blocks. Build Environ 2010;45(3):758-65.
[18] Mak CM, Yun Y. A study of power transmissibility for the vibration isolation of coherent vibratory machines on the floor of a building. Appl Acoust 2010;71(4):368-72.
[19] Yun Y, Mak CM. Power transmission from two coherent machines to a dual-layer coupling floor structure. J Vib Control 2011;17(5):711-20.
[20] Fuller CR. Noise-Control Characteristics of Synchrophasing, I: Analytical Investigation. AIAA J 1986;24(7):1063-8.

[21] Jones JD, Fuller CR. Noise-Control Characteristics of Synchrophasing, II: Experimental Investigation. AIAA J 1986;24(8):1271-6.
[22] Dench MR, Brennan MJ, Ferguson NS. On the control of vibrations using synchrophasing. J Sound Vib 2013;332(20):4842-55.
[23] Fahy FJ, Gardonio P. Sound and structural vibration: radiation, transmission and response. New York: Academic; 2007.
[24] ISO 7626-1:2011. Mechanical vibration and shock - Experimental determination of mechanical mobility - Part 1: Basic terms and definitions, and transducer specifications.
[25] ISO 7626-5:1994. Vibration and shock - Experimental determination of mechanical mobility - Part 5: Measurements using impact excitation with an exciter which is not attached to the structure.
[26] Tabassum M, Mathew K. A genetic algorithm analysis towards optimization solutions. Int J Digit Inf Wirel Commum 2014;4(1):124-42.